Partially-Saturated Brines Within Basal Ice or Sediments can Explain the Bright Basal Reflections in the South Polar Layered Deposits

David E Stillman[1], Elena Pettinelli[2], Sebastian Emanuel Lauro[3], Elisabetta Mattei[4], Graziella Caprarelli[5], Barbara Cosciotti[6], Katherine M. Primm[7], and Roberto Orosei[8]

[1]Southwest Research Institute
[2]Universita degli Studi Roma Tre
[3]Università Roma Tre
[4]Università degli Studi Roma TRE
[5]University of Southern Queensland
[6]Università di Roma TRE
[7]Planetary Science Institute
[8]Istituto Nazionale di Astrofisica

November 26, 2022

Abstract

Strong radar reflections have been previously mapped at the base of the Martian South Polar Layered Deposits (SPLD). Here, we analyze laboratory measurements of dry and briny samples to determine the cause of this radar return. We find that liquid vein networks consisting of brines at the grain boundaries of ice crystals can greatly enhance the electrical conductivity, thereby causing strong radar reflection. A liquid brine concentration of 2.7–6.0 vol% in ice is sufficient to match the electrical properties of the basal reflection as observed by MARSIS. When brine is mixed with sediments, we find that the brine-ice mixture in the pores must be 2–5 times more concentrated in salt, increasing the brine concentration to 6.3–29 vol%. Thus, our best fit of the median observed MARSIS value suggests a salt-bulk sample concentration of ~6 wt%, which is ~8 larger than that of the Phoenix landing site. To form brine, the basal reflector must reach a temperature greater than the eutectic temperature of calcium perchlorate of 197.3±0.2 K. Colder metastable brines are possible, but it is unclear if brines can remain metastable for millions of years. Additionally, grey hematite with a concentration of 33.2-59.0 vol% possess electrical properties that could cause the observed radar returns. However, such concentrations are 2-3 times larger than anywhere currently mapped on Mars. We also demonstrate that brines mixed with high-surface-area sediments, or dry red hematite, jarosite, and ilmenite cannot create the observed radar returns at low temperatures.

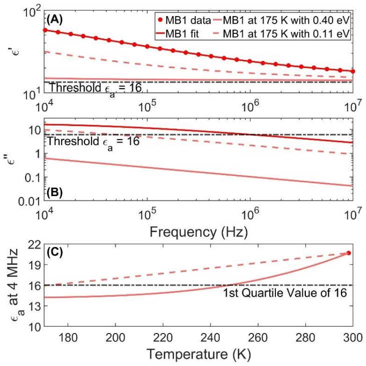

Figure S1. Real (**A**) part of the relative permittivity of the MB1 samples in *Rust et al.* (1999). MB1 is described as a glassy clast from a welded block and ash dacite breccia from Mount Meager, British Columbia, Canada. The data (red dots) were digitized from figure 5 in *Rust et al.* (1999). We then fit ε' with a Cole-Cole relaxation to find ε'' utilizing the Kramers-Kronig relationship (**B**) and then calculated ε_a (**C**). Activation energies E_a of 0.11 and 0.4 eV are then shown to estimate the activation energy of this anomalous low-frequency dispersion as estimated in *Stillman and Olhoeft* (2008) and *Stillman et al.,* (2010). At room temperature, the MB1 sample exceeds the observed 1st quartile value, however as temperature is decreased it drops below or matches the 1st quartile value depending on E_a.

Partially-Saturated Brines Within Basal Ice or Sediments can Explain the Bright Basal Reflections in the South Polar Layered Deposits

D.E. Stillman[1*] (dstillman@boulder.swri.edu), E. Pettinelli[2], S.E. Lauro[2], E. Mattei[2], G. Caprarelli[3], B. Cosciotti[2], K.M. Primm[4] and R. Orosei[5]

[1] Department of Space Studies, Southwest Research Institute, Boulder, USA
[2] Mathematics and Physics Department, Roma Tre University, Rome, Italy
[3] Centre for Astrophysics, Institute for Advanced Engineering and Space Sciences, University of Southern Queensland, Toowomba, Australia
[4] Planetary Science Institute, Tucson, AZ, USA
[5] Istituto di Radioastronomia (IRA), Istituto Nazionale di Astrofisica (INAF), Bologna, Italy

*Corresponding author

Submitted to: JGR-Planets

Initially Submitted: May 26, 2022

Key points:

- Brines within ice and icy sediments can explain the bright basal reflection in the south polar layered deposits
- Salt enhancements of 5–16 times the salt-regolith concentration at the Phoenix landing site is needed in brine-sediment mixtures
- Calcium perchlorate brines are stable above their eutectic temperature, which is experimentally measured at 197.3±0.2 K

Abstract

Strong radar reflections have been previously mapped at the base of the Martian South Polar Layered Deposits (SPLD). Here, we analyze laboratory measurements of dry and briny samples to determine the cause of this radar return. We find that liquid vein networks consisting of brines at the grain boundaries of ice crystals can greatly enhance the electrical conductivity, thereby causing strong radar reflection. A liquid brine concentration of 2.7–6.0 vol% in ice is sufficient to match the electrical properties of the basal reflection as observed by MARSIS. When brine is mixed with sediments, we find that the brine-ice mixture in the pores must be 2–5 times more concentrated in salt, increasing the brine concentration to 6.3–29 vol%. Thus, our best fit of the median observed MARSIS value suggests a salt-bulk sample concentration of ~6 wt%, which is ~8 larger than that of the Phoenix landing site. To form brine, the basal reflector must reach a temperature greater than the eutectic temperature of calcium perchlorate of 197.3±0.2 K. Colder metastable brines are possible, but it is unclear if brines can remain metastable for millions of years. Additionally, grey hematite with a concentration of 33.2–59.0 vol% possess electrical properties that could cause the observed radar returns. However, such concentrations are 2–3 times larger than anywhere currently mapped on Mars. We also demonstrate that brines mixed with high-surface-area sediments, or dry red hematite, jarosite, and ilmenite cannot create the observed radar returns at low temperatures.

Plain-Speak Abstract

Previously research has shown that strong radar reflections emanate from the interface between Mars' southern ice cap and their underlying sediments over a region with an area of 20×30 km and 1.5 kms beneath the surface. Radar reflections are caused by changes in electrical properties. Here, we analyze electrical property laboratory measurements of materials under Mars-like conditions. We find that a small amount (~3–6%) of brine in ice samples could create strong radar reflections similar to those that are observed. A greater concentration of salt is needed in sediment ice mixtures, such that a salt enhancement of ~10 would be needed compared to the rest of Mars. Additionally, a calcium perchlorate brine could only form if the temperature was greater than 197.3 K. Colder metastable brines are possible, but it is unclear if brines can remain metastable for millions of years. Additionally, dry grey hematite could also cause the observed radar returns, but the concentration of grey hematite would have to be 2–3 times larger than anywhere else on Mars.

We can also rule out any brines mixed with clays, or dry red hematite, jarosite, and ilmenite as they cannot create the observed radar returns at low temperature.

1. Introduction

The Mars Advanced Radar for Subsurface and Ionospheric Sounding (MARSIS) instrument on Mars Express has detected strong subsurface radar reflections in the region of Ultimi Scopuli (81°S, 193°E), within the South Polar Layered Deposits (SPLD) (*Orosei et al.*, 2018; *Lauro et al.*, 2021). These subsurface reflections are ~10 dB greater in power than the surrounding reflections and ~3 dB greater than the reflections from the surface (*Orosei et al.*, 2018). The reflecting unit is located at the base of the SPLD, approximately 1.5 km below the topographic surface. Because data acquired by MARSIS do not separate the real (ε') and imaginary (ε'') parts of the complex permittivity of reflectors, the apparent permittivity (ε_a), a single parameter accounting for both ε' and ε''(*Mattei et al.*, 2022a; ref. to §2.2) is commonly reported. In their investigation of the SPLD, *Orosei et al.* (2018) obtained reflectivities characterized by a median ε_a value of 33±1 at 4 MHz. Using a threshold value of ε_a = 15, the largest reflective zone is ~20×30 km (*Lauro et al.*, 2021). Furthermore, *Lauro et al.* (2021) also detected at least three other smaller locations, about 10 km across, within 120 km of the largest anomaly.

The high reflectivity values observed by MARSIS (*Orosei et al.*, 2018) were found to have a 1st and 3rd quartile values ε_a of 16 and 91, respectfully. Such high values of ε_a significantly limit the number materials that could cause such reflections. Three categories of materials have thus far been proposed to explain the high reflectivity values: clays with adsorbed water (*Smith et al.*, 2021); dry minerals and rocks with high iron content (*Bierson et al.*, 2021; *Grima et al.*, 2022); and saline ice (*Bierson et al.*, 2021).

Smith et al. (2021) suggested that the dielectric relaxation of clay with adsorbed water at the base of the SPLD could result in high ε_a values at the presumed basal temperature in Ultimi Scopuli. However, *Smith et al.*'s (2021) data were measured at 230 K and are inconsistent with similar types of measurements as reported in the literature (*Moore and Maeno*, 1993; *Stillman et al.*, 2010; *Stillman and Grimm*, 2011b; *Lorek and Wagner*, 2013; *Cunje et al.*, 2018; *Kułacz and Orzechowski*, 2019; *Mattei et al.*, 2022a).

Bierson et al. (2021) suggested that red hematite is a possible source for the bright reflection, because it has an ε' = 18.1 (*Robinson and Friedman*, 2003). In fact, *Robinson and Friedman* (2003) found that a soil sample of red hematite with 50.5% porosity, likely a reasonable analog for Martian soils, has a bulk ε'= 4.5, which is consistent with measurements reported by *Stillman and*

Olhoeft (2008). The ε' = 18.1 used by *Bierson et al.* (2021) was the estimate of the grain or solid permittivity, which assumes no porosity. Assuming minimal porosity of 10% for a hematite-rich rock, using *Robinson and Friedman's* (2003) mixing models we estimate a bulk ε' value of 10.8, which is lower than the observed 1st quartile value. As an alternative, the same authors also suggested jarosite as a possible material, based on its proposed high value of ε'. This is however inconsistent with dry soil measurements of permittivity for this mineral, as published in the literature (ref. to figure 1 in *Stillman and Olhoeft*, 2008).

Grima et al. (2022) suggested that measurements of bulk ε'>16 have been reported for ilmenite ($FeTiO_4$) and basalts (*Parkamento*, 1967; *Shmulevich et al.*, 1971; *Rust et al.*, 1999). We addressed this specific interpretation later on in this paper, where we present and discuss the results of our measurements on dry ilmenite.

Bierson et al. (2021) suggested that the conductivity of saline ice, i.e., ice with a bulk salt mass concentration range of 0.1–3.5 wt%, could return ε_a values observed at Ultimi Scopuli. Liquid brines have high ε'(~80) and are highly conductive; thus, brines in ice or sediments can plausibly create ε_a values within range of those observed by MARSIS (*Mattei et al.*, 2022a).

Here, we report on our experimental investigation of the compositional and thermal range of stability of Martian-consistent brines, which is the principal purpose of this study. We also address the dry material interpretation through our laboratory experiments on selected dry materials. The paper is structured as follows: (*i*) we briefly provide a background into the MARSIS instrument, electrical properties of materials, formation of brines, and estimated basal temperatures in Ultimi Scopuli (§2); (*ii*) we then present our measurement methodology (§3); (*iii*) we follow with a discussion of our results (§4); (*iv*) we then proceed to interpret our results in the context of published hypotheses on the nature of the reflectors (§5); and (*v*) our principal findings are summarized in the conclusions (§6).

2. Background

2.1 MARSIS

MARSIS acquires data on four channels, with center frequencies of 1.8, 3, 4, and 5 MHz, each with a bandwidth of 1 MHz (e.g., *Picardi et al.*, 2005). The MARSIS dataset used by *Orosei et al.* (2018) and *Lauro et al.* (2021) was acquired without onboard synthetic-aperture radar processing to ensure the amplitudes were as accurate as possible (*Lauro et al.*, 2021). These MARSIS results rely on the 4 MHz center frequency data as it is the most complete data set around the Ultimi Scopuli region (*Lauro et al.*, 2021). The radius of the first Fresnel zone is ~3.5-6 km depending on satellite altitude (300-800 km) (*Orosei et al.*, 2018), while the more conservative pulse limited criterion, has a diameter of 7.5 km assuming a satellite altitude of 400 km (*Lauro et al.*, 2021). Thus, the anomalous areas are larger than the pulse limited criterion. Lastly, the vertical resolution is ~55 m, after range compression and Hanning windowing when assuming an ε' = 3.1 of pure ice (*Lauro et al.*, 2021).

2.2 Electrical Properties

The electrical properties of the material control the speed at which radar waves propagate, the amount of energy that is attenuated, and how much energy is reflected at discontinuities. Here and in the following discussion, we ignore the effects of the magnetic permeability, given its small variability (*Stillman and Olhoeft*, 2008). The real part of the relative dielectric permittivity (ε') primarily controls the speed at which radar waves propagate through the material. In most dry rocks at radar frequencies, ε' can be estimated using the following equation:

$$\varepsilon' = (1.93 \pm 0.17)^{\rho}, \qquad \text{(Eq. 1)}$$

where ρ is the bulk density of the rock or soil in g cm^{-3} (*Olhoeft and Strangway,* 1975). The imaginary part of the relative dielectric permittivity (ε'') primarily controls the attenuation of radar waves through the material and is a summation of losses due to dielectric relaxations (ε''_p) and Direct Current (DC) electrical conductivity (σ_{DC}),

$$\varepsilon'' = \varepsilon''_p + \frac{\sigma_{DC}}{2\pi f \varepsilon_o}, \qquad \text{(Eq. 2)}$$

where *f* is the frequency of the radar energy and ε_o is the dielectric permittivity in vacuum (8.854 × 10^{-12} F m^{-1}).

Next, we convert ε' and ε'' into ε_a (*Mattei et al.*, 2022a) using

$$\varepsilon_a = \varepsilon_1 \frac{\varepsilon_1 + |\varepsilon_2| + \sqrt{\varepsilon_1^2 + |\varepsilon_2|^2 - 2\varepsilon_1 \varepsilon_2'}}{\varepsilon_1 + |\varepsilon_2| - \sqrt{\varepsilon_1^2 + |\varepsilon_2|^2 - 2\varepsilon_1 \varepsilon_2'}}, \qquad \text{(Eq. 3)}$$

where ε_1 is the ε' of the SPLD assumed to be 3.5, ε'' of the SPLD is assumed to be zero, and magnitude of the permittivity of the basal reflector is

$$|\varepsilon_2| = \sqrt{\varepsilon_2'^2 + \varepsilon_2''^2}. \qquad \text{(Eq. 4)}$$

In **Figure 1**, the combination of the reflector's ε'_2 and ε''_2 that would create ε_a similar to that observed in the MARSIS data at 4 MHz (*Lauro et al.*, 2021) is shown: minimum values of ε'_2 and ε''_2 of 13.5 and 6, respectively, could allow for an $\varepsilon_a \geq 16$, i.e., the observed 1st quartile value. If both the real and imaginary part values of a material are less than these minimum values, then ε_a cannot reach the MARSIS threshold values observed.

Electrical properties are frequency dependent because different polarization mechanisms separate charges at different speeds (e.g., *Stillman and Olhoeft*, 2008; *Stillman et al.*, 2010). To model the material's frequency dependence, we use the Cole-Cole equation (*Cole and Cole*, 1941, *Stillman and Olhoeft*, 2008). Frequency dependent, materials are also temperature dependent, because the speed at which charge separates is temperature dependent: this behavior is modeled with a Boltzmann temperature dependence (e.g., *Stillman and Olhoeft*, 2008, and refs. therein). These models allow us to extrapolate and interpolate electrical properties in frequency and temperature. Thus, ε' and ε'' measured to 1 MHz can be extrapolated to comprise the MARSIS frequency range of 2 – 5 MHz (e.g. *Stillman and Grimm*, 2011a). Additionally, as the frequency dependence shifts to lower frequency at colder temperatures, we can test whether the extrapolation is valid (*Stillman and Grimm*, 2011a).

2.3 Formation of Brines

Salt-H_2O mixtures are characterized by four distinct phases (**Fig 2A**):

(1) Brine: when the temperature of the mixture is above the melting temperature;

(2) Brine + ice: when the temperature of a sub-eutectic concentration (<49.8 wt% for $Ca(ClO_4)_2$) is below the melting temperature, but above the eutectic temperature;

(3) Brine + hydrate: when the temperature of a super-eutectic concentration is below the melting temperature, but above the eutectic temperature; and

(4) Ice + hydrate: when the temperature of a mixture is below the eutectic temperature.

Here, we focus on the brine + ice phase for sub-eutectic concentrations. As a sub-eutectic concentration (<49.8 wt% for $Ca(ClO_4)_2$) sample begins to freeze below the melting point, H_2O is fractionated out of the system as pure ice (or nearly pure ice if Cl^-, F^-, or NH_4^+; for more see *Gross et al.*, 1977; *Petrenko and Whitworth*, 1999; *Stillman et al.*, 2013ab) and the salt-H_2O mass concentration increases in the liquid brine until it reaches a eutectic concentration at the eutectic temperature. The amount of liquid brine present at the eutectic depends on its initial concentration and salt type (**Fig. 2**). For very low salt concentrations in the mixture, the melt accumulates at the boundaries of the ice grains. Even low salinity brines (e.g., ~3 mM, ~0.03 mass%, or ~0.06 vol%; *Grimm et al.*, 2008) are electrically conductive, they form electrically connected networks across the ice matrix, defined as along Liquid Vein Networks (LVNs). Thus, salt-H_2O mixtures display high electrical conductivity even when most of the ice is frozen (*Grimm et al.,* 2008; *Stillman et al.,* 2010). The electrical conductivity of the mixture drops significantly below the eutectic temperature, when the entire system is frozen.

2.4 Estimated Basal SPLD Temperature

Estimates of the values of SPLD basal temperatures in Ultimi Scopuli have been recently published (*Sori and Bramson*, 2019; *Ojha et al.,* 2019; *Egea-González et al.,* 2022), and are heavily dependent upon the heat flow from the planetary interior, and the thermal conductivity of the SPLD, both of which are not fully constrained. Assuming a temperature-dependent thermal conductivity of pure H_2O ice for the SPLD, a heat flow >84 mW/m^2 is required to allow liquid Ca-perchlorate brine to form. For a more realistic heat flow range of 14-25 mW m^{-2} (*Parro et al.,* 2017), a basal temperature of ~171-176 K is obtained (*Sori and Bramson*, 2019). *Egea-González et al.* (2022) found a basal temperature range of 175-187 K using the maximum surface heat flow (32 mW m^{-2}) by assuming a dust proportion of 15%. We speculate that inclusion of CO_2 ice into H_2O ice layers or as pure CO_2 layers within the SPLD could further enhance basal temperatures (*Wiezorek*, 2008), as CO_2 ice has a thermal conductivity that is 5-6 times lower than that of H_2O ice (e.g., *Mellon*, 1996).

3. Methods

This section describes the methodology of electrical property measurements of salt-H_2O mixtures and salt-H_2O mixtures with Martian analogs. Note, new measurements are complemented by data obtained in previous published (*Grimm et al.,* 2008; *Stillman et al.,* 2010; *Stillman and Grimm*, 2011ab) and unpublished work. Low-frequency measurements were conducted at Southwest Research Institute in Boulder Colorado. Solutions of salt-H_2O mixtures were freshly prepared before each measurement. For measurements of salt-H_2O mixtures, the liquid solution was poured into the three-electrode sample holder with a Teflon cup (Solartron 12962A and 12964A). For measurements of salt-H_2O mixtures with Martian analogs, the analogs (e.g., clays, sands, ilmenite) were dried in a vacuum at ~1 mbar and ~383 K until their mass changed by less than 0.5% over a ~12-hour period. The granular analog material was then spooned into the Teflon cup sample holder with a spatula, then the liquid solution was poured into the granular material. Lastly, the sample was intimately mixed with a spatula to ensure a homogenous sample was created. The sample was 3.5 cm in diameter and ~0.6 cm thick. The sample holder was then placed into the sample chamber.

The sample chamber has been previously described (*Grimm et al.,* 2008; *Stillman et al.,* 2010). For measurements made after Sept 2019, we used a custom vacuum chamber that is placed in the Ultra-Low freezer (So-Low C85-9). Only dry materials were measured in vacuum of ~1 mbar, samples with ice were measured at atmospheric pressure. The sample holder sits on a liquid nitrogen cold plate so that temperatures below 180 K can be obtained. Lake Shore Cryotronics Silicon diode (DT-670) temperature sensors are used to measure the sample temperature on the Teflon cup and a second sensor controls two 25 W cartridge heaters (Lake Shore HTR-25-100) via a Lake Shore Cryotronics temperature controller (331). The sample is then connected via BNC cables to a Solartron 1260A impedance analyzer and a Solartron 1296A dielectric interface. The sample temperature was then lowered to reach a temperature that is 2 K below its freezing point for 1 hour to initialize crystallization. Subsequently, the temperature is further decreased to 10 K below the freezing point for an additional 2 hours to ensure crystallization of any metastable water. Reheating of the sample is carried out by raising the temperature back to 2 K below the freezing point for 3 hours. This process guarantees formation of stable LVNs for the entire duration of the experiment, reducing the rate of cracking in the sample, and avoiding the effect of rapid recrystallization. The temperature of the sample is then drastically lowered at a rate the is lower or equal to <1 K min^{-1} to the sample's lowest temperature. Electrical property measurements are conducted non-stop as soon as the sample obtains properties that allow it to be measured easily, typically this occurs when σ_{DC} < 0.1 S/m. After obtaining the lowest temperature value the sample is slowly heated. To increase temperature accuracy, the target temperature is held to within 0.2 K for at least 20 min. Typically, measurements are made over the range of 1–10^6 Hz, which takes ~6 minutes to acquire. However, as σ_{DC} increases the lower frequency limit is also increased, which reduces the time required to measure a spectrum. Additionally, once the sample reaches the frequency at which σ_{DC} dominates the electrical properties the uncertainly of ε' increases greatly.

The electrical property measurements output complex impedance as a function of frequency, which is converted into complex dielectric permittivity using the electrode geometry. Cole-Cole parameters of each spectrum were modeled by nonlinear curve fitting (*Stillman and Olhoeft*, 2008; *Grimm et al.*, 2008; *Stillman and Grimm*, 2011ab). The Cole-Cole parameters were then used to find ε_a at 4 MHz as a function of temperature.

4. Results and Interpretations

4.1 Dry Ilmenite

Dry granular ilmenite (purchased from Ward's Scientific) with 35.5% porosity and a bulk density of 3.07 g cm^{-3} possesses a significant σ_{DC} and a polarization mechanism that increases ε' and ε'' at MARSIS frequencies (**Fig. 3**). The observed relaxation mechanism is known as an anomalous low-frequency dispersion (e.g., *Jonscher* 1978; 1999; *Shahihi et al.*, 1975; *Stillman et al.*, 2010). Previously reported data indicate that ilmenite reaches a value of $\varepsilon' > 33$ at room temperature (*Parkmenko*, 1967). In our experiments, at ~273 K, the ε_a of ilmenite does not approach the observed median, dropping below the observed 1st quartile value at a temperature of ~252.8 K. Therefore, we conclude that ilmenite is not a plausible candidate as the cause of the strong basal reflections at Ultimi Scopuli.

4.2 Chloride Salt-H_2O Mixtures

Chloride brines in ice were previously shown to obtain high values of σ_{DC} and ε'' at temperatures above their eutectic temperatures (*Grimm et al.*, 2008). However, NaCl (*Grimm et al.*, 2008) and $MgCl_2$ (*Primm et al.*, 2020) have eutectic temperatures of 251 and 240 K, respectively; thus, they are too high to be considered in the context of the SPLD. $CaCl_2$ has a much lower eutectic temperature of 223 K (*Stillman et al.*, 2010). The ε_a data versus temperature and concentration show that a 100 mM (1.1 wt%) of $CaCl_2$ at the eutectic temperature has an ε_a equivalent to the observed 1st quartile value (**Fig. 4**). The ε_a of the 1,000 mM (10 wt%) of $CaCl_2$ is larger than the observed 3rd quartile value (**Fig. 4**), indicating a lower concentration is need to match the 3rd quartile value.

4.3 Perchlorate Salt-H_2O Mixtures

Because of their low eutectic temperatures of 198 and 216 K (*Toner et al.*, 2014) respectively, calcium and magnesium perchlorate brines have been proposed as most plausible source for the bright basal reflections in Ultimi Scopuli (*Lauro et al.*, 2021). The ε_a versus temperature and concentration show that a concentration of 100 mM (2.2 wt%) of $Mg(ClO_4)_2$ is just below the observed 1st quartile value (**Fig. 5**), while 500 mM (10 wt%) of $Mg(ClO_4)_2$ is greater than the observed 3rd quartile value (**Fig. 5**).

For the 300 mM (6.9 wt%) of $Ca(ClO_4)_2$, the selected measurements of ε' (**Fig. 6A**) and ε'' (**Fig. 6B**) display a strong ice relaxation below the eutectic temperature. Above the eutectic temperature, σ_{DC} increases to large values (**Fig. 6C**) so that ε' can no longer be measured accurately due to so much energy being dissipated by ε''. The observed dependence of ε_a with temperature demonstrates that concentrations of 300 mM (6.9 wt%) of $Ca(ClO_4)_2$ are sufficient to obtain the observed 3rd quartile value at the measured eutectic temperature of 197.3±0.2 K (**Fig. 7**). The brine in the 200 mM (4.7 wt%) of $Ca(ClO_4)_2$ never frozen into hydrate and ice even though the temperature was dropped to 161.9 K. As will be shown in the next section and **Figure 8**, ε_a has the same value at a given temperature when above the eutectic temperature no matter whether the temperature is warming or cooling. Thus, ε_a at the eutectic temperature for the 200 mM $Ca(ClO_4)_2$ sample shows it is near the median observed value, making this a likely material for the base of the SPLD in Ultimi Scopuli. Meanwhile, the 100 mM (2.4 wt%) $Ca(ClO_4)_2$ sample shows it is below the 3rd quartile value.

4.4 Metastability of Salts-H_2O Mixtures

The results of the experiments conducted to explore the metastability of perchlorate brines are shown in **Figure 8**. For the 300 mM (6.7 wt%) $Ca(ClO_4)_2$, the brine remained in a metastable form down to a temperature of 187.9±0.2 K, i.e., 9.4 K below the eutectic temperature, although the measured value of ε_a is below the observed 1st quartile. The decreasing value of ε_a with decreasing temperature is attributed to a decreasing volume of the liquid brine combined. Thus we conclude that, to record values of apparent permittivity consistent with the bright MARSIS reflections, metastable brines must form from concentrations above that in this experiment. We were able to hold the brine sample in a metastable form for 6.9 hours before decreasing the temperature to a lower temperature. Metastability of other salts has been previously reported to last at least 72 hours when held at a temperature a few degrees below the eutectic temperature (*Primm et al.*, 2020). Other $Ca(ClO_4)_2$ samples displayed in **Figures 7 & 9** never froze even though they were taken to temperatures below 173 K.

4.5 Salt-H_2O Mixtures in Low-Surface Area Sediments

Previous measurements (*Stillman et al.*, 2010) have shown that brines in low-specific-surface (<1 m^2/g) area sediments also show distinct increases of σ_{DC} at the eutectic temperature that indicate that LVNs still dominate conduction in icy sediment mixtures. Our experiments were conducted with fine-grained (mean grain size of 110 μm) sand with a porosity of ~40%. We focused on $Ca(ClO_4)_2$ salt-H2O mixture with sand. We found that a 37.8 vol% of 700 mM (15.1 wt%) $Ca(ClO_4)_2$ mixed with sand is near the observed ε_a values for the 1st quartile (**Fig. 9**). Similarly, a 40.4 vol% of 1.5 mM (29.1 wt%) $Ca(ClO_4)_2$ mixed with sand is near the observed ε_a values for the median observed values (**Fig. 9**), making this a likely material for the base of the SPLD in Ultimi Scopuli.

4.6 Salt-H_2O Mixtures in High-Surface Area Sediments

Clay samples from the Clay Mineral Society were previously measured at Mars-like temperatures (*Stillman et al.*, 2010; *Stillman and Grimm*, 2011ab). A compilation of multiple samples of STx-1 (Texas Calcium Montmorillonite) measured dry and with slight additions of water at a temperature of 193.2±0.2 K are shown in **Figure 10**. STx-1 possesses a large H_2O surface area of 217 m^2/g (*Jänchen et al.*, 2009), where 3 and 7 monolayers (ML) represent ~14 and ~32 wt% water, respectively. (Note a ML of water was assumed to be 0.3 nm thick.) None of the data plotted approach the ε_a threshold for the 1st quartile observations. Furthermore, the full temperature dataset for 7 ML of 100 mM $CaCl_2$ indicates that, once the temperature drops below 233 K, the electrical properties are not compatible with the 1st quartile MARSIS observations (**Fig. 11**).

For this work, we measured clay specimen SAz-1 ("Cheto" from Arizona with an N_2 surface area of 97.4 m^2/g) saturated with 54.2 wt% of 500 mM $Ca(ClO_4)_2$ brine (**Fig. 12**). While the sample displays σ_{DC} and strong polarization mechanisms, these are not of sufficient magnitude to approach the range of ε_a values observed by MARSIS. Thus, our new experiment corroborates the conclusion that salt-H_2O mixtures in high-surface area sediments do have increased values of σ_{DC}

above the eutectic temperature (*Stillman et al.,* 2010; *Mattei et al.,* 2022ab). While absorbed/bound water does conduct electrical current below and above the eutectic temperature, the ions in adsorbed/bound water are less mobile and follow a much more tortuous path compared to brines in sand or ice (*Stillman et al.,* 2010; 2019).

JSC Mars-1, which consists of hematite and titano-magnetite, has been measured by many researchers (e.g., *Williams and Greeley,* 2004; *Stillman and Olhoeft*, 2008). When measured dry, it does not approach the 1st quartile values. JSC Mars-1 has a large H_2O surface area (106 m^2/g; *Pommerol et al.,* 2009) due to a palagonitic surface. However, even with 7 ML (~18 wt%) it still does not obtain large electrical property values approaching the range of ε_a values of that observed by MARSIS until temperatures larger than 273 K (**Fig. 13**). In conclusion, salt-H_2O mixtures in high-surface area (>1 m^2/g) sediments do not possess a large enough σ_{DC} to provide an ε_a value at SPLD-like temperatures that is similar to the bright reflector measured by MARSIS.

5. Discussion

5.1 Dry Minerals

A discussion on red hematite and jarosite is not necessary as previous measurements in the literature can eliminate these minerals, as was discussed in §2.5. While dry ilmenite can have very high ε_a values at room temperature (*Parkmenko*, 1967; *Boivin et al.,* under review), temperature dependence significantly lowers ε_a values (**Fig. 3**). Thus, ilmenite has an ε_a value near ~12 that is lower than the observed 1st quartile value at the approximate temperature of the base of the SPLD.

Intrusive and extrusive igneous rocks were measured by *Shmulevich et al.* (1971) of which 12 of 89 had $\varepsilon' > 13.5$ at 500 MHz, which could have an $\varepsilon_a > 16$ depending on their ε'', which were not published. There is little data regarding the methodology of the *Shmulevich et al.* (1971) measurements. Leaving many important questions: what temperature were the samples measured at, where the samples were acquired, and were the samples vacuum or thermally dried or measured as collected? Additionally, frequency and temperature dependence are also omitted. Thus, it is impossible to extrapolate these measurements to SPLD temperatures and MARSIS frequencies given the lack of details given in *Shmulevich et al.* (1971).

Many other measurements (*Campbell and Ulrichs*, 1969; *Chung et al.*, 1970; *Gold et al.*, 1970; *Adams et al.,* 1996; *Russell and Stasiuk,* 1997) of volcanic rocks all measured $\varepsilon' < 12$ at radar frequencies. While *Rust et al.* (1999) found two of 34 basaltic samples, with an $\varepsilon' > 13.5$ at 4 MHz and at room temperature. Only the MB1 sample has an ε_a > 16 at 4 MHz at room temperature (**Fig. S1**). *Rust et al.* (1999) does comments that this sample hosts thin cracks, thus a layer of absorbed water could be increasing ε' as has been measured by many other (e.g., *Jonscher* 1978; 1999; *Shahidi et al.*, 1975; *Knight and Endres*, 1990; *Stillman et al.*, 2010). Thus, we are skeptical that this single basalt measurement could produce an ε_a value due to adsorbed/bound water that is larger than clay or JSC Mars-1.

Grey hematite possesses a radio-frequency relaxation with a small activation energy of 0.1 eV (*Stillman and Olhoeft*, 2008). A dry sample of 59.0 vol% grey hematite with a porosity of 41.0% can obtain the median MARSIS ε_a value at 4 MHz over possible SPLD-like temperatures (**Fig. 14**). This is a significant amount of grey hematite and about four times greater than the maximum grey hematite value measured at the surface of 15% at Aram Chaos and Meridiani Planum (*Glotch and Christensen*, 2005). Additionally, the grey hematite in Meridiani Planum is a lag deposit and thus concentrated compared to its *in-situ* formation concentration (*Hynek*, 2004). This is likely why no large increases in surface reflectivity have been measured at Aram Chaos or Meridiani Planum even though they have a high surficial concentration of grey hematite.

To further explore the possibilities of grey hematite, we perform dielectric mixing models. Using a Licktenecker power law mixing formula (*Stillman and Olhoeft*, 2008), we estimate the solid grain ε_a of grey hematite to be 137.6 at 4 MHz at 200 K, assuming a grain density δ_G of 5.26 g cm^{-3}. We then used *Eq. 1* to estimate an ε_a value of ultramafic and mafic grain assuming a δ_G of 3.8 and 3.0 g cm^{-3}, respectively. We assume that any porosity is filled with ice (no brine) with ε_a of 3.15 as ground ice is stable below the SPLD. We then created four mixing models with grey hematite (**Fig. 15; Table 1**) using a power-law mixing model with an exponent of 2.65 (*Shabtaie and Bentley*, 1994; *Stillman et al*., 2010). First, we mix grey hematite with ice that produces grey hematite volume concentrations of 26.8-45.2-81.0% for the observed 1st quartile-median-3rd quartile values. The replacement of the porosity with ice reduces the volume concentration of the median value from 59.0% (**Fig. 15**) to 45.2%, however this is still three times larger than the largest values detected on the surface of Mars. We then assume an ice-filled porosity of 19% and 10%, while mixing the ultramafic grains with grey hematite. This produces smaller grey hematite concentrations of 12.4-35.6-81.0% and 10.0-33.2-78.6% for ice concentrations of 19% and 10%, respectively, for the observed 1st quartile-median-3rd values. These values of grey hematite are only about two times larger than those detected on the surface, however the bulk density δ_B of these mixtures are higher than any typical volcanic rocks measured on Earth (*Olhoeft and Johnson*, 1984; *Shmulevich et al.*, 1971; *Kiefer et al.*, 2012; *Rust et al.*, 1999). To reduce δ_B, we then mixed a 10% ice with grey hematite and mafic grains to produce grey hematite concentrations of 18.5-39.2-79.8%. Such a reduction in δ_B leads to an increase in grey hematite concentration, and would likely still produce a measurable gravity anomaly. *Li et al.* (2012) displays no gravity anomaly is present at the Ultimi Scopuli site, albeit greater gravity resolution is needed before this could be totally ruled out. Overall, we find that large amounts of grey hematite can create ε_a values that match the MARSIS observations. However, the concentration of grey hematite (median values from 33.2-59.0 vol% and 3rd quartile value from 78.6-81.0 vol%) and extent (20-30 km ellipse) of the deposits needed rival that of terrestrial banded iron formation, such formations are not expected on Mars.

5.2 Metastability and Premelting

Measurements made while cooling brine mixtures can show significant hysteresis as well as long-term (of at least a few days) stability (**Fig. 8**; *Primm et al.,* 2020). Unlike the measurements of $MgCl_2$ (*Primm et al.*, 2020), we could not reproduce the metastability of $Ca(ClO_4)_2$. One experiment froze as low as 188 K, while many other experiments it did not freeze down to 173 K and in one case down to 163 K. Recall, *Toner et al.* (2014) measured two $Ca(ClO_4)_2$ samples, which did not freeze until 153 K. Without freezing no hysteresis was measured. It is far from demonstrated that the longevity of metastable brines shown in laboratory settings extends over geologic timescales. Therefore, below we pursued hypotheses that do not require metastability until future improved temperature models can fully eliminate the possibility of SPLD basal temperatures of 197.3 K.

Figures 5, 6, & 7 show an increase in ε_a and σ_{DC} before the eutectic temperature is reached. This parabolic behavior is known as premelting (e.g., *Rempel et al.*, 2004; *Stillman et al.*, 2010; 2019; *Rempel*, 2012) and is typically seen in terrestrial permafrost samples as they approach their melting temperature near 273 K (*Grimm and Stillman,* 2015). This premelting effect allows very high salt concentrations to reach the observed MARSIS ε_a values a degree or two below the salt's eutectic temperature.

5.4 Brine Mixtures

Partially-saturated brines are capable of increasing ε_a to the observed values, if the temperature is greater than the eutectic temperature of the salt (**Figs 4, 5, & 7**). The significant increase in ε_a is due to the increase in ε'' via σ_{DC}. Our $Ca(ClO_4)_2$-H_2O measurements show that 1st and 3rd quartile values are reached at the eutectic temperature with a $Ca(ClO_4)_2$ concentration of 140 mM (3.3 wt%) and 310 mM (7.1 wt%), respectively (**Fig. 16**). Note, the lower end of this range overlaps with the upper range of saline ice (0.1–3.5 wt%) range, as suggested by *Bierson et al.* (2021). The bulk brine concentrations of these samples at the 1st and 3rd quartile values are 2.7 and 6.0 vol% brine at a eutectic temperature (**Fig. 2**).

In salt-H_2O-sediment mixtures, the salt-H_2O just occupies the pore space. Thus, a greater concentration of salt is needed when mixed with sediment to match the MARSIS observations compared to the salt-H_2O mixtures without sediment. At the eutectic temperature, we find that for a mixture that is ~60 vol% sand and 40 vol% $Ca(ClO_4)_2$-H_2O the observed ε_a values for the 1st and 3rd quartile values would have a $Ca(ClO_4)_2$ concentration of 770 mM (16.4 wt%) and 2.5 M (43.4 wt%), respectively (**Fig. 16**). We then modeled the amount of brine in the bulk sample to calculate a brine concentration of 6.3 and 28.7 vol% at the 1st and 3rd quartile values, respectively. Thus, we find that the brine concentration in fine sand must be 2-5 times larger than when the brine is just in ice. This occurs because of increased tortuosity of the LVNs, which leads to a lower σ_{DC}. This drop in σ_{DC} is much larger when the pores and pore throats are even smaller. Therefore, high-specific surface area sediments (i.e., clays and JSC Mars-1) possess LVNs, but with high tortuosity and small σ_{DC} (*Stillman et al.,* 2010; 2019; *Stillman and Grimm,* 2011ab; **Figs. 10-13**) Therefore, these salt-H_2O-sediment mixtures cannot obtain the MARSIS observed ε_a values.

5.5 Salt Enhancement

The salt-regolith concentration discovered at the Phoenix landing site was 0.7 mass% (*Hecht et al.*, 2009). Our 1st quartile, median, and 3rd quartile salt-H_2O-sediment values have a salt-bulk sample concentration of 3.6, 5.7, and 11.3 mass%, respectively. Thus, the sediment at the basal layer of the SPLD would have to be enhanced by a factor of ~5–16 compared to the Phoenix landing site. Below we discuss four salt enhancement mechanisms:

(1) Drainage of an interconnected system of LVNs could drain concentrate brine down through the SPLD. Similar physics occurs within sea ice and has been hypothesized to occur within the

Europa ice shell (e.g., *Hesse et al.*, 2022). LVNs could have drained to the base of the SPLD or have drained into regolith/rock sediments below the SPLD.

(2) The sublimation of CO_2/H_2O snow from a previous SPLD-like construct would have left deposited salt on the remaining sediment or dust upon which the current SPLD now rests. Similar processes occur when snow with small amount of salt blows into the upper dry valleys in Antarctica. This snow then sublimates away, leaving the sediment highly enriched in salt (*Levy et al.,* 2012).

(3) The sublimation of ice due to a change in orbital parameters can concentrate the amount of dust and by proxy the amount of salt mixed into the dust. This process has occurred in the SPLD as images at the edge of the SPLD show layers with varying amount of dust (some likely with more than 10%; *Milkovich and Plaut*, 2008). Note that ~80% of the ice would have to sublimate here to concentrate the ice to our estimated values, as such the resulting layer would be more similar to a salt-H_2O mixture in sediments.

(4) Salt could also be concentrated via the accumulation of water in a paleolake, which then dried up, concentrating salts in the paleolake sediments. Similar processes are thought to have formed the chloride deposits found throughout the southern highlands (*Osterloo et al.*, 2008). Note that these previously identified deposits have a maximum area of 25 km^2 compared to the strong reflector that has an area of ~600 km^2.

6. Conclusions

Here, we have compiled new and old measurements of electrical properties of Martian analog materials at SPLD basal temperatures. This paper has shown that of all the materials proposed as the source of the bright reflections at Ultimi Scopuli, only brine-rich ice mixtures are viable options. $Ca(ClO_4)_2$ brines are the most likely brine as they have the lowest eutectic temperature of any common Martian salt. The concentration of $Ca(ClO_4)_2$ to H_2O needed is 140 – 310 mM (3.3 – 7.1 mass%) to obtain the observed 1st and 3rd quartile values. Likewise if liquid brines exist in sediment with ~40% porosity, a larger concentration of 0.77 – 2.5 M (16.4 – 43.4 mass%) of $Ca(ClO_4)_2$ is required to obtain the observed 1st and 3rd quartile values. Thus, the sediments require a factor of ~5-16 concentration in salt enhancement compared to that measured at the Phoenix landing site. However, the large increase by $Ca(ClO_4)_2$ brines is only stable above its measured eutectic temperature of 197.3±0.2 K, which is too large estimates of simple SPLD thermal models.

We suggest that layers of CO_2 ice or CO_2 mixed in with H_2O could increase the basal temperatures above the eutectic temperature of $Ca(ClO_4)_2$. Additionally, the volume of brine is estimated to be 2.7-6.0 vol% and 6.3-28.7 vol% in ice mixtures and sand mixed ice, respectively. Thus, partially-saturated ice or ice sediment mixtures (not briny lakes) are required to produce the observed reflection.

If thermal modeling cannot increase temperatures to the eutectic temperature of $Ca(ClO_4)_2$, then metastable brines are necessary to drop the range at which brines could exist. However, additional research is needed constrain the stability/lifetime of metastable brines, as well as a larger concentration of salt. We also demonstrated that grey hematite is the only known mineral on Mars to possess a large ε_a when dry and at SPLD-like temperatures. However, concentrations 2–4 times (33.2–59.0 vol%) than any currently known are needed to match the MARSIS SPLD observations. Such large concentrations of grey hematite would produce a gravity anomaly that could be used to test this hypothesis.

Acknowledgments. We acknowledge the support of the space agencies of Italy (ASI) and the United States (NASA) for the development and science operations of MARSIS. Operations of the Mars Express spacecraft by the European Space Agency (ESA) are gratefully acknowledged. D.S. was supported by NASA grant #80NSSC20K0858. The authors thank Luca Guallini, Francesco Soldovieri, and Robert Grimm for intellectual discussions regarding this subject. D.S. thanks Michael Shoffner for his laboratory assistance. Data for this paper can be found here DOI: 10.5281/zenodo.6600729

References

Adams, R.J., Perger, W.F., Rose, W.I., Kostinski, A., (1996) Measurements of the complex dielectric constant of volcanic ash from 4 to 19 GHz. *J. Geophys. Res. 1*, 8175–8185.

Bierson, C.J., Tulaczyk, S., Courville, S.W., Putzig, N.E., (2021). Strong MARSIS radar reflections from the base of Martian south polar cap may be due to conductive ice or minerals. *Geophys. Res. Lett.*, e2021GL093880.

Boivin, A.L., C-A. Tsai, D.C. Hickson, R.R. Ghent, M.G. Daly (under review) Determination of Broadband Complex EM Parameters of Powdered Materials Part B: Ilmenite-Bearing Lunar Analogue Materials, *J. Geophys. Res.*

Campbell, M.J., Ulrichs, J., (1969) Electrical properties of rocks and their significance for lunar radar observations. *J. Geophys. Res. 25*, 5867–5881.

Chung, D.H., Westphal, W.B., Simmons, G., (1970). Dielectric properties of Apollo 11 lunar samples and their comparison with earth materials. *J. Geophys. Res. 75*, 6524–6531.

Cole, K. S., and Cole, R. H. (1941), Dispersion and Absorption in Dielectrics: *The Journal of Chemical Physics*, *9*, 341 – 351.

Cunje, A.B., R.R. Ghent, A. Boivin, C.A. Tsai, D. Hickson, (2018) Dielectric properties of Martian regolith analogs and smectite clays. *Lunar Planet. Sci. Conf.*, #2083.

Egea-González, I., P.C. Lois, A. Jiménez-Díaz, et al., (2022) The stability of a liquid-water body below the south polar cap of Mars, *Icarus*, in press, https://doi.org/10.1016/j.icarus.2022.115073

Glotch, T. D., and P. R. Christensen (2005), Geologic and mineralogic mapping of Aram Chaos: Evidence for a water-rich history, *J. Geophys. Res., 110*, E09006, doi:10.1029/2004JE002389.

Gold, T., Campbell, M.J., O'Leary, B.T., (1970) Optical and high-frequency electrical properties of the lunar sample. *Science 167*, 707–709.

Grima, C., Mouginot, J., Kofman, W., Hérique, A., & Beck, P. (2022). The basal detectability of an ice-covered Mars by MARSIS. *Geophysical Research Letters, 49*, e2021GL096518. https://doi.org/10.1029/2021GL096518

Grimm, R.E., Stillman, D.E., (2015) Field Test of Detection and Characterisation of Subsurface Ice using Broadband Spectral-Induced Polarisation, *Permafrost and Periglac. Process.*, *26*, 28–38, DOI: 10.1002/ppp.1833.

Grimm, R.E., Stillman, D.E., Dec, S.F., Bullock, M.A., (2008). Low-frequency electrical properties of polycrystalline saline ice and salt hydrates. *J. Phys. Chem. B112* (48), 15382–15390.

Grimm, R.E., Stillman, D.E., J.A. MacGregor (2015) Dielectric signatures and evolution of glacier ice, J. Glaciology, 61(230) 1159-1170. doi: 10.3189/2015JoG15J113

Gross, G.W., Wong, P.M. and Humes, K. (1977) Concentration dependent solute redistribution at the ice-water phase boundary. III. Spontaneous convection. Chloride solutions. *J. Chem. Phys., 67(11)*, 5264–5274.

Robinson, D. A., Friedman, S. P. (2003). A method for measuring the solid particle permittivity or electrical conductivity of rocks, sediments, and granular materials. *Journal of Geophysical Research, 108,* 2076. https://doi.org/10.1029/2001JB000691

Hecht, M.H., et al. (2009) Detection of Perchlorate and the Soluble Chemistry of Martian Soil at the Phoenix Lander Site, *Science 325*, 64 DOI: 10.1126/science.1172466.

Hesse, M.A., J.S. Jordan, S.D., Vance, and A.V. Oza (2022) Downward oxidant transport through Europa's ice shell by density-driven brine percolation, *Geophysical Research Letters, 49*, e2021GL095416. https://doi.org/10.1029/2021GL095416

Hynek, B. (2004) Implications for hydrologic processes on Mars from extensive bedrock outcrops throughout Terra Meridiani. *Nature 431***,** 156–159. https://doi.org/10.1038/nature02902

Jänchen, J., D. L. Bish, and U. Hellwig (2009), The H2O sorption properties of a martian dust analog, *40th Lunar and Planetary Science Conference*, The Woodlands, TX, March 23-27, #1395.

Jonscher, A. K. (1978) Low-Frequency Dispersion in Carrier-Dominated Dielectrics, Philos. Mag. B., 38, 587-601.

Jonscher, A. K. (1999) Dielectric Relaxation in Solids, *J. Phys. D: Appl. Phys.*, *32*, R57-R70.

Kiefer, W. S., R. J. Macke, D. T. Britt, A. J.Irving, and G. J. Consolmagno (2012), The density and porosityof lunar rocks,Geophys. Res. Lett.,39, L07201, doi:10.1029/2012GL051319.

Knight, R.J., Endres, A., (1990) A new concept in modeling the dielectric response of sandstones: defining a wetted rock and bulk water system. *Geophysics 55*, 586–594.

Kułacz, K., K. Orzechowski, (2019) Nontronite and intercalated nontronite as effective and cheap absorbers of electromagnetic radiation, *Dalton Transactions, 48(12)*, 3874-3882.

Lalich, D.E., A.G. Hayes, V. Poggiali (2021) Explaining Bright Radar Reflections Below the Martian South Polar Layered Deposits Without Liquid Water, arXiv, uploaded Jul, 7, 2021 https://doi.org/10.48550/arXiv.2107.03497

Lauro, S.E., Pettinelli, E., Caprarelli, G., Guallini, L., Rossi, A.P., Mattei, E., Orosei, R., (2021). Multiple subglacial water bodies below the south pole of Mars unveiled by new MARSIS data. Nat. Astron. 5(1), 63–70.

Levy, J. S., A. G. Fountain, K. A. Welch, and W. B. Lyons (2012), Hypersaline "wet patches" in Taylor Valley, Antarctica, *Geophys. Res. Lett., 39*, L05402, doi:10.1029/2012GL050898.

Li, J., J. C. Andrews-Hanna, Y. Sun, R. J. Phillips, J. J. Plaut, and M. T. Zuber (2012), Density variations within the south polar layered deposits of Mars, *J. Geophys. Res.*, *117*, E04006, doi:10.1029/2011JE003937.

Lorek, A., N. Wagner (2013) Supercooled interfacial water in fine-grained soils probed by dielectric spectroscopy. *The Cryosphere*, *7(6)*, 1839-1855.

Mattei, E., E. Pettinelli, S.E. Lauro, D.E. Stillman, B. Cosciotti, L. Marinangeli, A.C. Tangari, F. Soldovieri, R. Orosei and G. Caprarelli, (2022a). Assessing the role of clay and salts on the origin of MARSIS basal bright reflections at Ultimi Scopuli, Mars, *Earth Planet. Sci. Lett.*, *579*, 117370.

Mattei, E., A. Brin, B. Cosciotti, S.E. Lauro, E. Pettinelli, G. Caprarelli, D.E. Stillman, L. Colantuono, L. Marinangeli, A.C. Tangari. (2022b) Dielectric properties of clays at MARSIS frequency and Martian temperature, *Lunar Planet. Sci Conf*, The Woodlands, Mar 7-11, #1392.

Mellon, M.T. (1996) Limits on the CO2 content of the martian polar deposits. *Icarus 124*, 268–279.

Milkovich, S. M., and J. J. Plaut (2008), Martian South Polar Layered Deposit stratigraphy and implications for accumulation history, *J. Geophys. Res.*, *113*, E06007, doi:10.1029/2007JE002987.

Moore, J.C., N. Maeno, (1993) Dielectric properties of frozen clay and silt soils. *Cold Regions Science and Technology*, *21(3)*, 265-273.

Ojha, L., Karimi, S., Buffo, J., Nerozzi, S., Holt, J. W., Smrekar, S., & Chevrier, V. (2021). Martian mantle heat flow estimate from the lack of lithospheric flexure in the south pole of Mars: Implications for planetary evolution and basal melting. *Geophysical Research Letters*, *48*, e2020GL091409. https://doi.org/10.1029/2020GL091409

Olhoeft, G. R., and D. W. Strangway (1975), Electrical properties of the first 100 meters of the moon, Earth Planet. Sci. Lett., 24, 394–404.

Olhoeft, G.R., and G.R. Johnson (1984) in Robert S. Carmichael (ed.), Handbook of Physical Properties of Rocks, vol. III, CRC Press, Inc.

Orosei, R., Lauro, S.E., Pettinelli, E., Cicchetti, A., Coradini, M., Cosciotti, B., Seu, R., (2018). Radar evidence of subglacial liquid water on Mars. Science 361 (6401), 490–493.

Osterloo, M.M., V.E. Hamilton, J.L. Bandfield, T.D. Glotch, A.M. Baldridge, P.R. Christensen, L. L Tornabene, F.S. Anderson (2008) Chloride-Bearing Materials in the Southern Highlands of Mars, *Science, 319*, 1651-1654. DOI: 10.1126/science.1150690

Parkhomenko, E.I., (1967). Electrical Properties of Rocks.

Parro, L. M., Jiménez-Díaz, A., Mansilla, F., & Ruiz, J. (2017). Present-day heat flow model of Mars. *Nature Scientific Reports, 7(1)*, 45629. https://doi.org/10.1038/srep45629

Petrenko, V. F. and R. W. Whitworth (1999), Physics of Ice. 1st ed., Oxford Univ. Press.

Picardi, G., et al. (2005), Radar sounding of the subsurface of the Mars, *Science, 310*, 1925–1928, doi:10.1126/science.1122165.

Pommerol, A., B. Schmitt, P. Beck, and O. Brissaud (2009), Water sorption on Martian regolith analogs: Thermodynamics and near-infrared reflectance spectroscopy, *Icarus, 204,* 114–136, doi:10.1016/j.icarus.2009.06.013.

Primm, K.M., Stillman, D.E., Michaels, T.I., (2020). Investigating the hysteretic behavior of Mars-relevant chlorides. Icarus 342, 113342.

Rempel, A.W., (2012). Hydro-mechanical processes in freezing soils. *Vadose Zone J.,* 11. http://dx.doi.org/10.2136/vzj2012.0045.

Rempel, A.W., Wettlaufer, J.S., Worster, M.G., (2004). Premelting dynamics in a continuum model of frost heave. *J. Fluid Mech. 498, 227–244*. http://dx.doi.org/10.1017/S0022112003006761.

Russell, J.K., Stasiuk, M.V., (1997) Characterization of volcanic deposits with ground penetrating radar. *Bull. Volcanol. 58*, 515–527.

Rust, A., Russell, J., & Knight, R. (1999). Dielectric constant as a predictor of porosity in dry volcanic rocks. *Journal of Volcanology and Geothermal Research, 91(1*), 79–96. https://doi.org/10.1016/s0377-0273(99)00055-4

Shabtaie, S. and C.R. Bentley (1994) Unified theory of electrical conduction in firn and ice: Site percolation and conduction in snow and firn, *J. Geophys. Res., 99*, 19,757-19,769.

Shahidi, M., Hasted, J. B., Jonscher, A. K. (1975) Electrical Properties of dry and humid sand, *Nature*, *258*, 595-597.

Shmulevich, S.A., Troitskiy, V.S., Zelinskaya, M.R., Markov, M.S., Sukhanov, A.L., 1971. Dielectric properties of rocks at a frequency of 500 MHz. Earth Phys. 12, 68–76.

Smith, I.B., Lalich, D., Rezza, C., Horgan, B., Whitten, J.L., Nerozzi, S., Holt, J.W., (2021). A solid interpretation of bright radar reflectors under the Mars south polar ice. *Geophys. Res. Lett.,* e2021GL093618.

Sori, M.M., Bramson, A.M., (2019). Water on Mars, with a grain of salt: local heat anomalies are required for basal melting of ice at the south pole today. *Geophys. Res. Lett. 46(3)*, 1222–1231.

Stillman, D., Olhoeft, G., (2008). Frequency and temperature dependence in electro-magnetic properties of Martian analog minerals. J. Geophys. Res., Planets 113 (E9).

Stillman, D.E., Grimm, R.E., (2011a). Radar penetrates only the youngest geological units on Mars. J. Geophys. Res., Planets 116 (E3).

Stillman, D.E., Grimm, R.E., (2011b). Dielectric signatures of adsorbed and salty liquid water at the Phoenix landing site, Mars. J. Geophys. Res., Planets 116 (E9).

Stillman, D.E., Grimm, R.E., Dec, S.F., (2010). Low-frequency electrical properties of ice – silicate mixtures. J. Phys. Chem. B114 (18), 6065–6073.

Stillman, D.E., J.A. MacGregor and R.E. Grimm, (2013a), The role of acids in electrical conduction through ice, *J. Geophys. Res., 118,* 1-16, doi:10.1029/2012JF002603.

Stillman, D.E., MacGregor, J.A., Grimm, R.E., (2013b). Electrical response of ammonium-rich water ice. Ann. Glaciol.54 (64), 21–26.

Stillman, D. E., K. P. Primm, S. L. Codd, J. D. Seymour, P. Lei, H. G. Sizemore, R. E. Grimm, A. W. Rempel (2019) Magnetic Resonance and Dielectric Spectroscopy Investigations of Liquid Vein Networks within Ice and Ice-Regolith Mixtures, *Lunar Planet. Sci. Conf.,* Mar 18-22, #2537.

Toner, J.D., Catling, D.C., Light, B., (2014). The formation of supercooled brines, viscous liquids, and low-temperature perchlorate glasses in aqueous solutions relevant to Mars. *Icarus 233*, 36–47.

Wieczorek, M.A., (2008) Constraints on the composition of the martian south polar cap from gravity and topography. *Icarus 196*, 506–517.

Williams, K. K. and R. Greeley (2004), Measurements of dielectric loss factors due to a Martian dust analog, *J. Geophys. Res., 109*, E10006, doi:10.1029/2002JE001957.

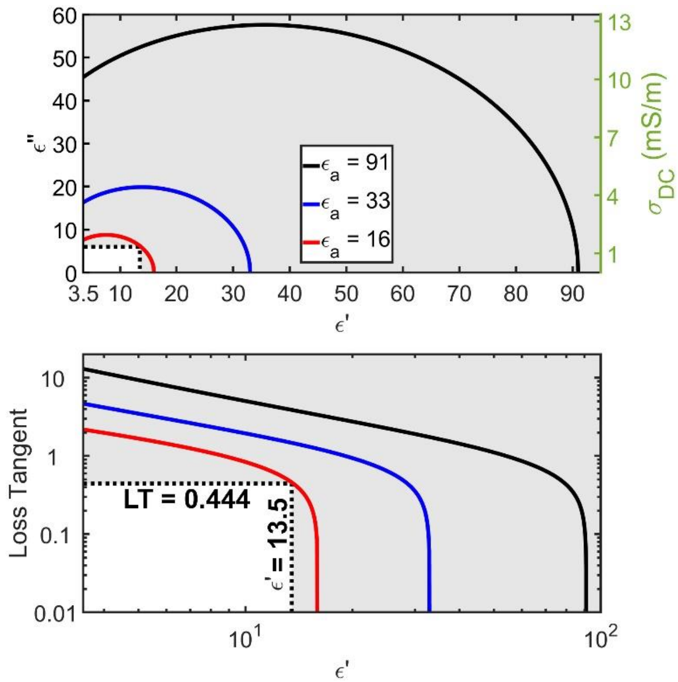

Figure 1. The solid lines display possible **(A)** ε' and ε'' and **(B)** ε' and loss tangent ($\varepsilon''/\varepsilon'$) that will combine for an ε_a equal to the 1st, 2nd (median), and 3rd quartile observed values of 16, 33, and 91, respectively. If a laboratory sample has a measured ε' and ε'' value of <13.5 and <6 (loss tangent of 0.444) at 4 MHz, respectively, then ε_a cannot obtain the 1st quartile MARSIS observed ε_a value. Note we assumed an ε' and ε'' of 3.5 and 0 for the SPLD. Additionally, the right y-axis in **(A)** shows the necessary values of σ_{DC}, if we assume all losses are conductive. Thus, σ_{DC} must be >1.3 mS m^{-1} to obtain the 1st quartile MARSIS observed ε_a value.

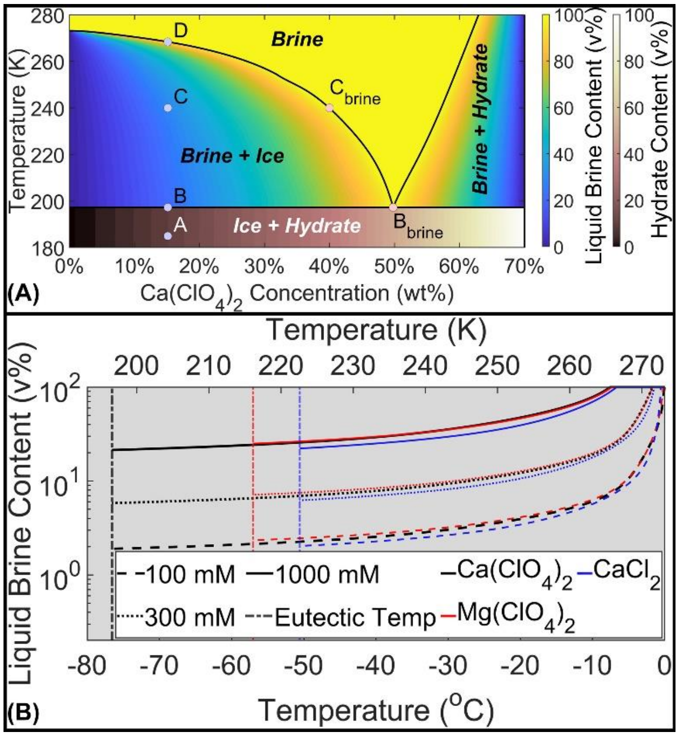

Figure 2. (A) Phase diagram of $Ca(ClO_4)_2$ with colored contours of bulk brine (parula colormap) and hydrate (pink colormap) concentrations. For example, a 700 mM (15.1 wt%) $Ca(ClO_4)_2$ sample at 185 K (Point A) has a hydrate content of ~12 vol%. At the eutectic temperature, the hydrate and ice melts to form a brine with a eutectic concentration (Point B_{brine}) and with a liquid content of ~14 vol%. At 240 K, the amount of liquid brine in the salt-H_2O mixture is ~22% (Point C), while the brine concentration is 40 wt% (Point C_{brine}). The sample then completely melts at 268.4 K (Point D). **(B)** Volume percent of brine at 100, 300, and 1000 mM versus temperature. The eutectic temperatures for $Ca(ClO_4)_2$, $Mg(ClO_4)_2$, and $CaCl_2$ are ~197.3, 216, 223 K, respectively.

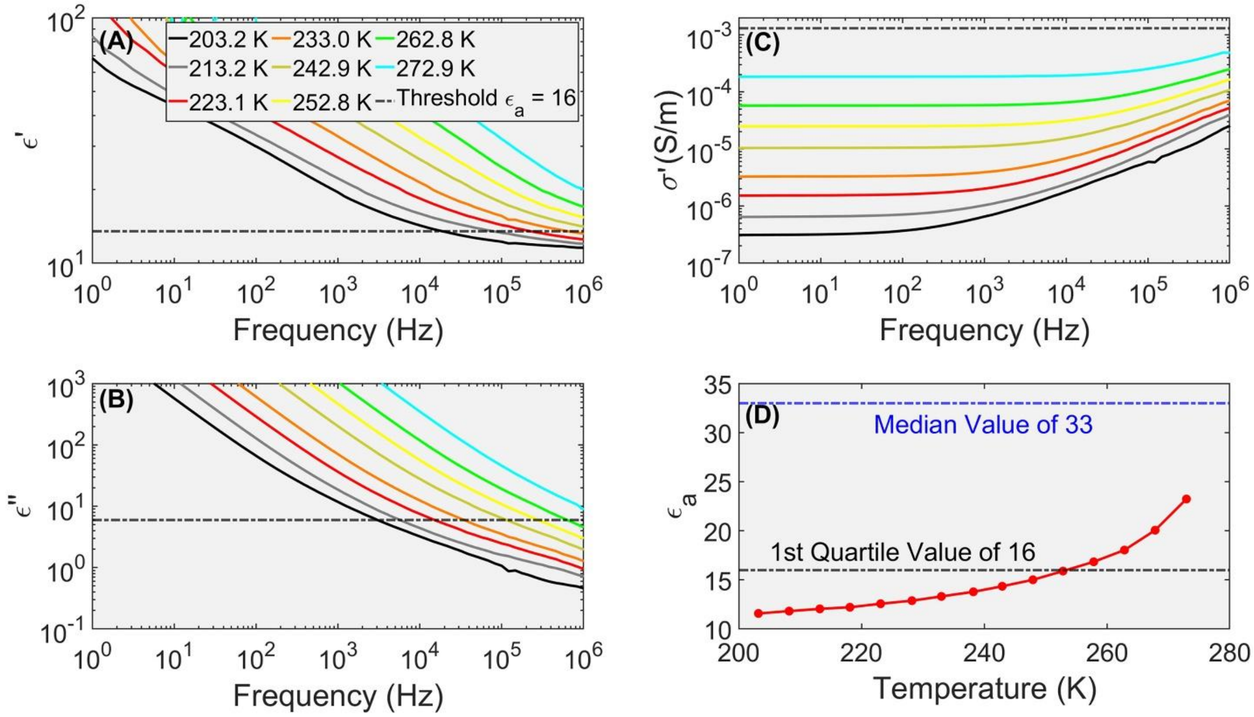

Figure 3. Real (**A**) and imaginary (**B**) part of the relative permittivity, real part of electrical conductivity (**C**) of ilmenite with 35.5% porosity. Ilmenite does have additional polarization mechanisms as well as σ_{DC} (shown by the plateau of σ' at low frequencies). The apparent permittivity (**D**) is calculated assuming an SPLD with $\varepsilon' = 3.5$ as a function of temperature. This shows that the polarizations and σ_{DC} are not large enough to produce ε_a values within the observed range at temperatures below ~252.8 K.

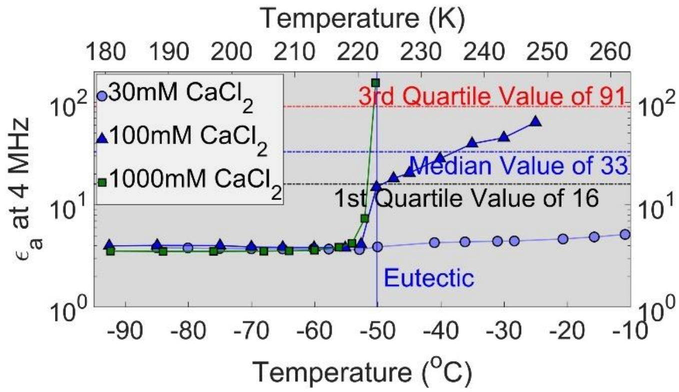

Figure 4. Apparent permittivity of various concentrations of $CaCl_2$ as a function of temperature. Of these concentrations, 100 mM (1.1 wt%) $CaCl_2$ is near the 1st quartile value of the observed MARSIS ε_a at 233 K.

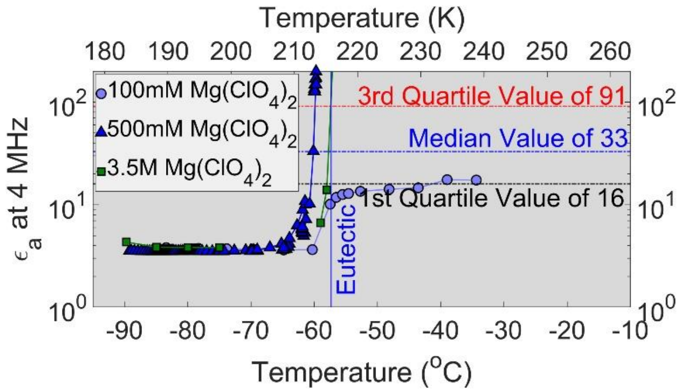

Figure 5. Apparent permittivity of various concentrations of $Mg(ClO_4)_2$ as a function of temperature. Of these concentrations, 100 mM (2.2 wt%) $Mg(ClO_4)_2$ is not able to obtain the 1st quartile value of the observed MARSIS ε_a at 216 K, while 500 mM (10 wt%) and 3.5 M (44 wt%) $Mg(ClO_4)_2$ possesses an ε_a that are larger than the 3rd quartile value above the eutectic temperature.

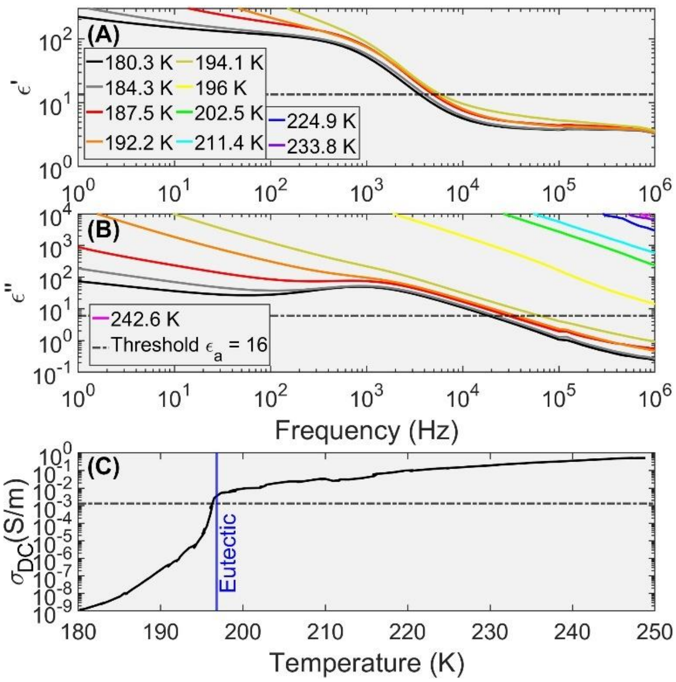

Figure 6. Real (**A**) and imaginary (**B**) part of the relative permittivity, and modeled DC conductivity (**C**) of 300 mM (6.9 wt%) $Ca(ClO_4)_2$ as a function of temperature. (**A** and **B**) show spectrum at selected temperatures, while (**C**) shows all the spectrum fitted over the entire measurement run. Note below the eutectic temperature the sample shows a dielectric relaxation of ice, however once the eutectic is reached the sample becomes conductive and ε' is not shown as it has little accuracy as all the energy is being dissipated conductively.

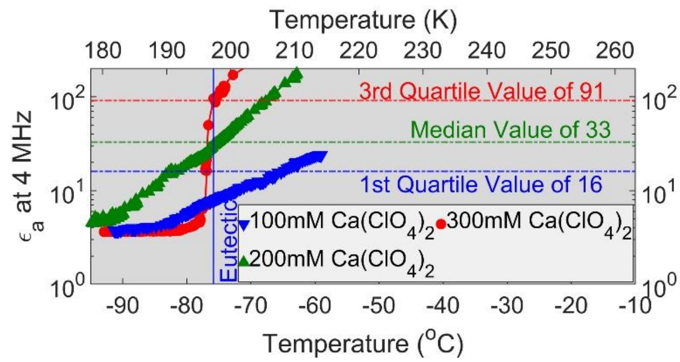

Figure 7. Apparent permittivity of mixtures as a function of temperature. The 200 mM (4.7 wt%) and 300 mM (6.9 wt%) $Ca(ClO_4)_2$ samples are near the observed median and 3rd quartile value at temperatures greater than the eutectic, respectively. The 100 mM (2.4 wt%) $Ca(ClO_4)_2$ sample is below the 1st quartile value. Note the 100 and 200 mM samples never froze, thus the values below the eutectic temperature are for a metastable brine.

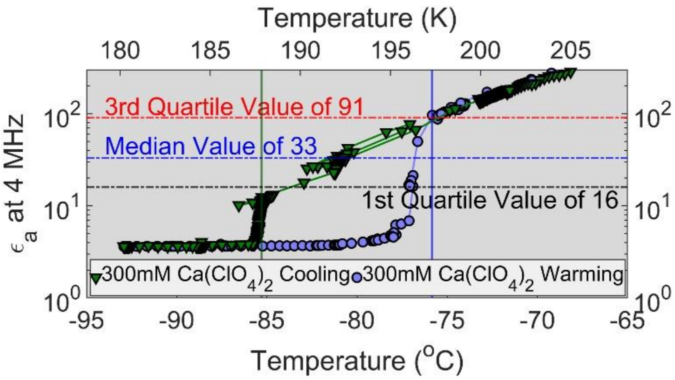

Figure 8. Apparent permittivity of 300 mM (6.9 wt%) $Ca(ClO_4)_2$ as a function of temperature for cooling and warming measurements. Note that the ε_a continues it constant decrease with temperature as it is cooled below the eutectic temperature, the brines in this sample then froze at a temperature of 187.9 K (vertical green line). Upon warming the brines then fully thaw at the eutectic temperature of 197.3 K (vertical blue line) and reach the same ε_a as during cooling.

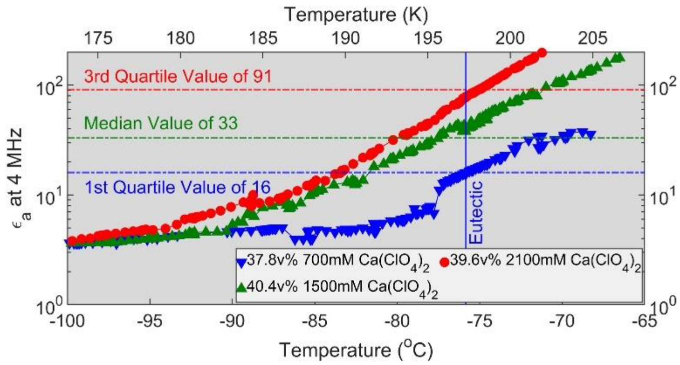

Figure 9. Fine-grained sand mixed with salt-H_2O mixtures of $Ca(ClO_4)_2$. Samples of 700 mM (15.1 wt%), 1.5 M (29.1 wt%), and 2.1 M (38.1 wt%) $Ca(ClO_4)_2$ are near the 1st quartile, median, and 3rd quartile values of ε_a, respectively, at the eutectic temperature of $Ca(ClO_4)_2$. Note that the displayed data do not possess the eutectic temperature jump indicative of melting. Thus, indicating that the $Ca(ClO_4)_2$ never froze even when lowered to below 173 K. Warming cycles (shown) and the cooling cycle (not shown for simplicity) show no hysteresis, further suggesting the brine is metastable below the eutectic temperature.

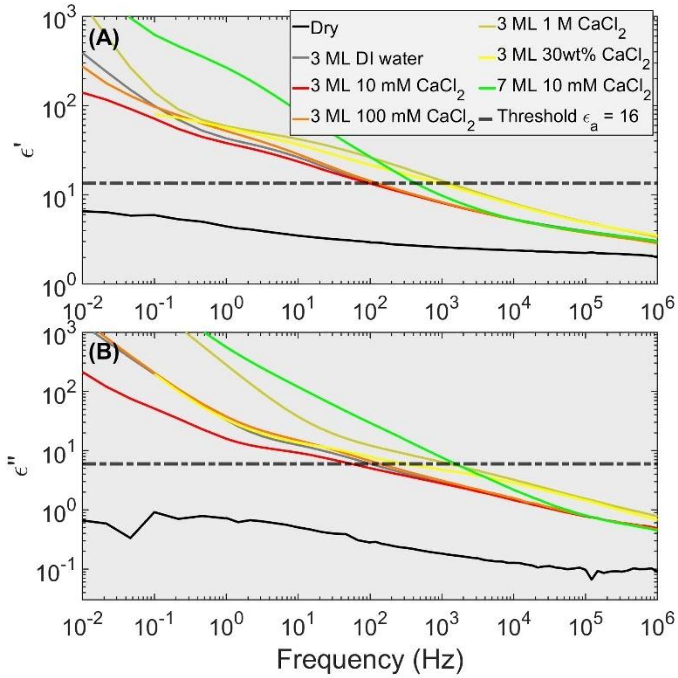

Figure 10. Compilation of ε' (**A**) and ε'' (**B**) values of dry and low-saturation measurements of Texas Calcium Montmorillonite (STx-1) at ~193.2±0.2 K, where ML is the number of calculated monolayers. At this temperature, the samples show no enhanced ε' or ε'' that could explain the MARSIS observed values measurements.

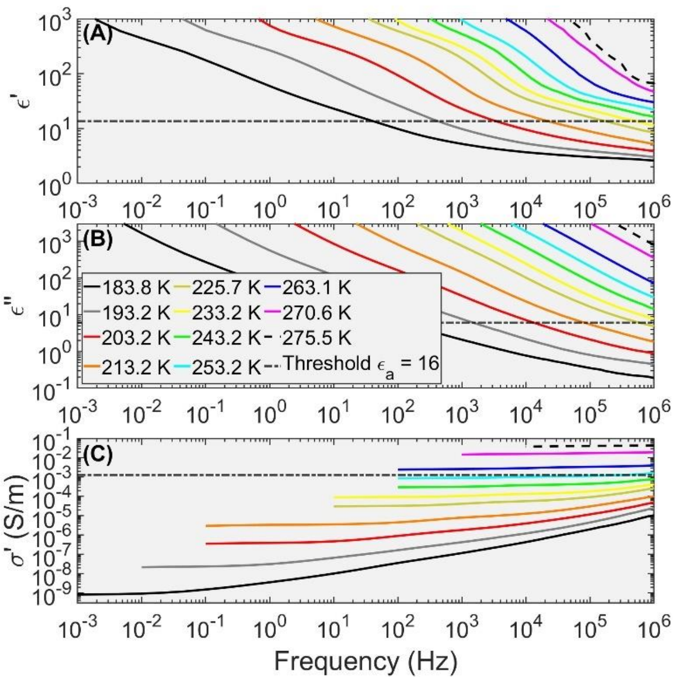

Figure 11. STx-1 measurements with 7 ML 100 mM (1.1 wt%) $CaCl_2$ for ε' (**A**), ε'' (**B**), and σ' (**C**). This sample had a STx-1, 100 mM $CaCl_2$, and air mass (volume) concentration of 70.4 mass% (28.0 vol%), 29.6 mass% (32.4 vol%), and 0 mass% (39.6 vol%), respectively. At 1 MHz, the electrical properties cannot obtain the ε_a threshold when temperatures are <233 K.

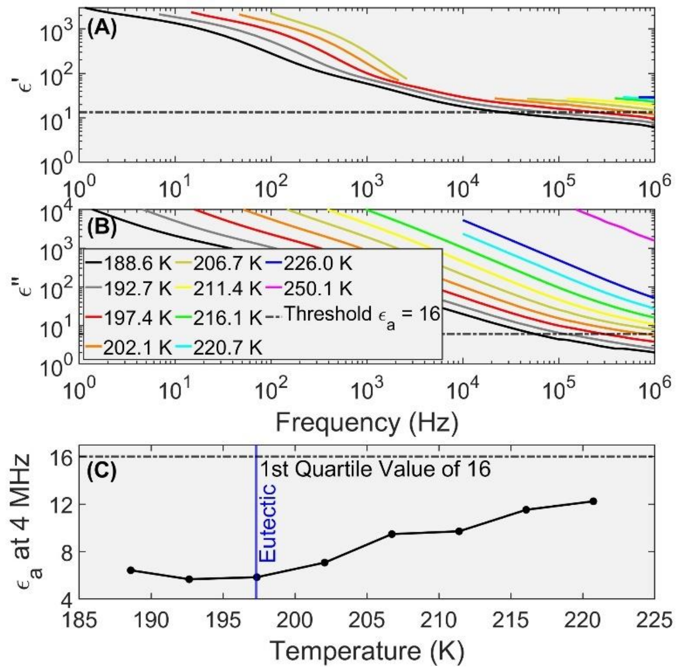

Figure 12. Complex electrical property measurements SAz-1 saturated with 500 mM (11.2 wt%) $Ca(ClO_4)_2$ with a mass (volume) concentration of 45.8 mass% (25.5 vol%) sand and 54.2 mass% (74.5 vol%) of salt-H_2O. (**A**) ε', (**B**) ε'', and (**C**) ε_a of the mixture shows that the sample has low-frequency broad dielectric relaxations and high DC conductivity, but never approaches the observed 1st quartile value.

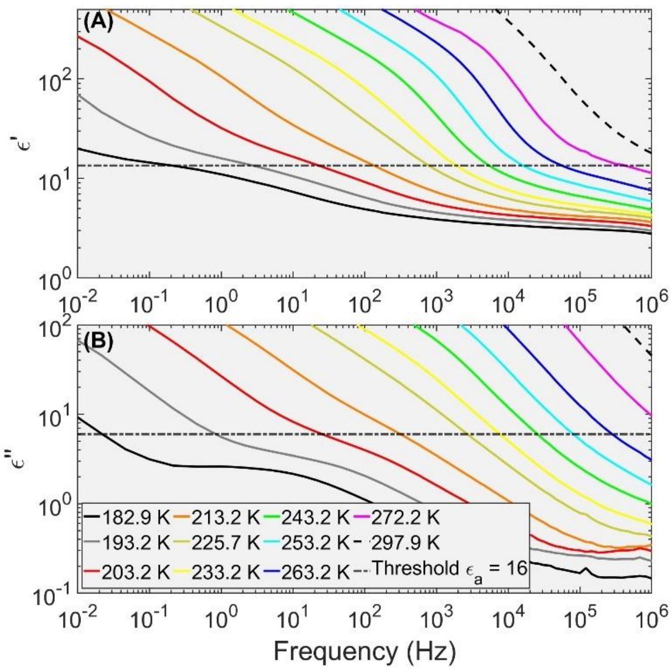

Figure 13. Complex electrical property measurements of JSC Mars-1 with 7 ML of 100 mM (1.1 wt%) $CaCl_2$. JSC Mars-1, 100 mM $CaCl_2$, and air in this partially-saturated sample had a mass (volume) concentration of 82.2 mass% (43.3 vol%), 17.8 mass% (17.9 vol%), and 0 mass% (38.8 vol%), respectively. The electrical properties do not approach the ε_a threshold for the 1st quartile value until the sample becomes completely unfrozen (>273 K). Thus, even with multiple polarization mechanisms of adsorbed water and ice combined with DC conductivity cannot approach the observed MARSIS threshold.

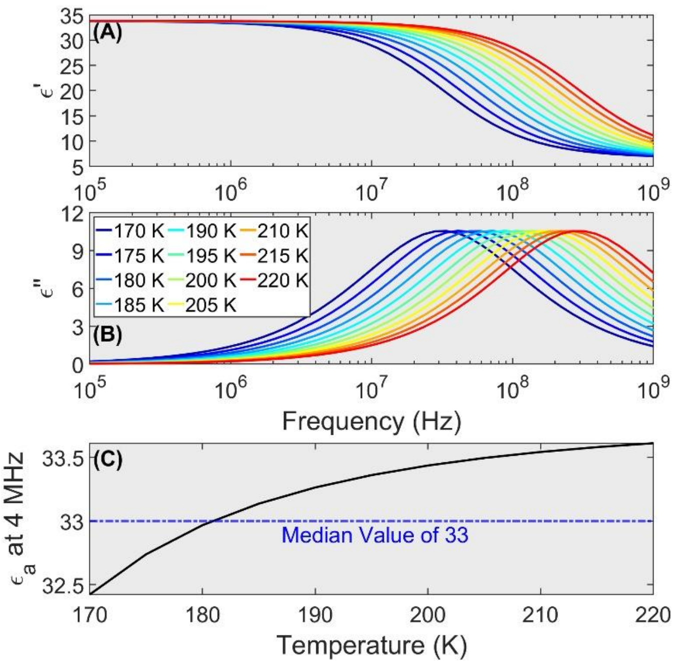

Figure 14. Electrical properties of grey hematite based on radar measurements modeled by *Stillman and Olhoeft* (2008). Note this model represent the measured sample that had a porosity of 41% and a grey hematite volume concentration of 59%. This high-frequency relaxation does not greatly affect ε_a at 4 MHz over typical SPLD temperatures.

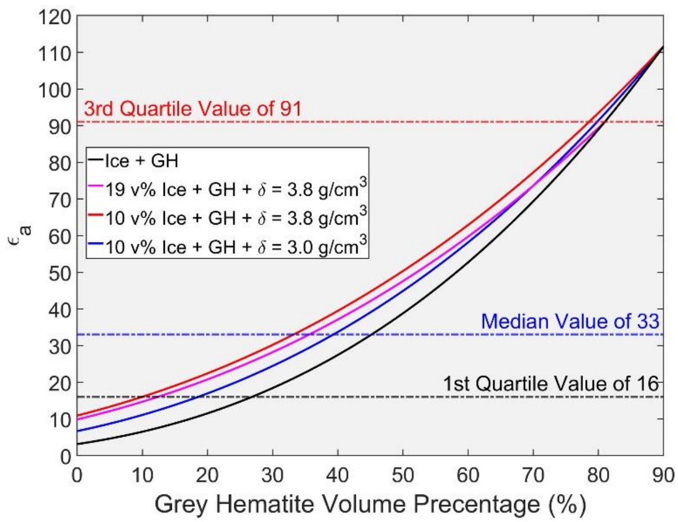

Figure 15. Four grey hematite (GH) mixing models are used to estimate the concentrations of ice, GH at 200 K, ultramafic (density δ = 3.8 g cm^{-3}) and mafic (δ = 3.0 g cm^{-3}) grains that would match the observed MARSIS ε_a values. Precise values are given in **Table 1**.

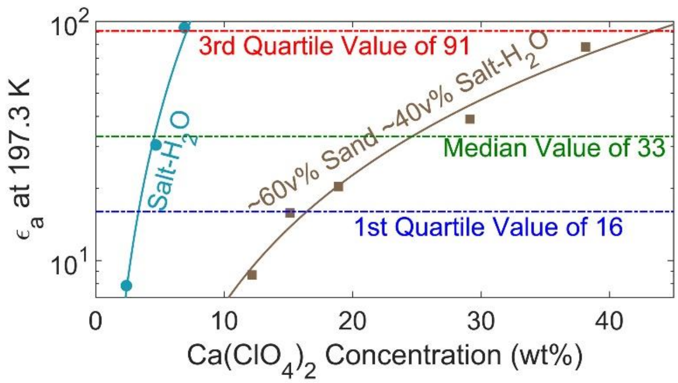

Figure 16. Apparent permittivity at the eutectic temperature versus calcium perchlorate mass concentration. The three experiments (symbols) of the salt-H_2O mixtures were fit (solid line) with a power law to calculate the 1st quartile, median, and 3rd quartile values of 3.3, 4.6, and 7.1 wt%, respectively. The five experiments of the sand mixtures with salt-H_2O were similarly fit with a power law to calculate the 1st quartile, median, and 3rd quartile values of 16.4, 24.6, and 43.4 wt%, respectively.

Table 1. Values of the four grey hematite (GH) mixing models shown in **Figure 15** at the observed 1st and 3rd quartile and median values of ε_a. The grain density δ_G values of 3.8 and 3.0 g cm^{-3} were used to represent an ultramafic and mafic grain density, respectively, and converted to permittivity using Eq 1. A δ_G of 5.26 and 0.917 g cm^{-3} were used for GH and ice, respectively, to calculate the bulk density δ_B. Note we assume that all pore space is filled by ice as ground ice should be stable under the SPLD. We also calculate δ_B by neglecting the contribution of ice to allow us to compare to terrestrial δ_B of rocks. In the comment's column, we assume that any rocks with a δ_B larger than 3.5 g cm^{-3} are too high (the largest density of the volcanic samples measured by *Rust et al.* (1999) and *Schmulevich et al.* (1971) was a gabbro at 3.39 g cm^{-3}). Additionally, we commented that any solution with a GH concentration greater than 30 vol% was too large as TES spectroscopic observations detected a maximum of 15 vol% of GH over Aram Chaos and Meridiani Planum (*Glotch and Christensen*, 2005).

ε_a	Ice	GH	δ_G = 3.8 g cm^{-3}	δ_G = 3.0 g cm^{-3}	δ_B g cm^{-3}	δ_B g cm^{-3} when replace ice with air	Comments
91	19.0%	81.0%			4.43	4.26	High density; Significant vol% of GH
33	54.8%	45.2%			2.87	2.37	Significant vol% of GH
16	73.2%	26.8%			2.08	1.41	Possible
91	19.0%	81.0%	0.0%		4.43	4.26	High density; Significant vol% of GH
33	19.0%	35.6%	45.4%		3.77	3.60	High density; Significant vol% of GH
16	19.0%	12.4%	68.6%		3.43	3.26	Possible
91	10.0%	78.6%	11.4%		4.66	4.57	High density; Significant vol% of GH
33	10.0%	33.2%	56.8%		4.00	3.90	High density; Significant vol% of GH
16	10.0%	10.0%	80.0%		3.66	3.57	High density
91	10.0%	79.8%		10.2%	4.59	4.50	High density; Significant vol% of GH
33	10.0%	39.2%		50.8%	3.68	3.59	High density; Significant vol% of GH
16	10.0%	18.5%		71.5%	3.21	3.12	Possible